Classification: Evolutionary Biology

Evolutionary analyses unveil the molecular mechanism of fast inactivation in calcium-permeable TRP channels

Lisandra Flores-Aldama[1,2,3], Michael W. Vandewege[4], Kattina Zavala[5], Charlotte K. Colenso[1], Daniel Bustos[6], Wendy Gonzalez[3,6], Sebastian E. Brauchi[1,3]*, Juan C. Opazo[5]*

[1]Instituto de Fisiología, Facultad de Medicina, Universidad Austral de Chile. [2]Programa de Doctorado en Ciencias mención Biología Celular y Molecular, Escuela de Graduados, Facultad de Ciencias, Universidad Austral de Chile. [3]Millennium Nucleus of Ion Channels-associated Diseases (MiNICAD). [4]Department of Biology, Eastern New Mexico University, Portales New Mexico, USA. [5]Instituto de Ciencias Ambientales y Evolutivas, Facultad de Ciencias, Universidad Austral de Chile, Valdivia. [6]Center for Bioinformatics and Molecular Simulations (CBSM) University of Talca, Talca.

Abbreviated Title: "The evolution of fast inactivation in calcium-selective TRP channels"

* Correspondence should be addressed to:

Juan C. Opazo: jopazo@gmail.com

Sebastian E. Brauchi: sbrauchi@uach.cl

Keywords: TRPV5; TRPV6; Gene Family Evolution; gene duplication

Abstract

Fundamental for calcium homeostasis in vertebrates, TRPV5 and TRPV6 are calcium-selective ion channels belonging to the Transient Receptor Potential (TRP) gene family. Detailed phylogenetic analysis suggests that duplications from which TRPV5 and TRPV6 originated occurred independently in the ancestors of mammals, sauropsids, amphibians, and chondrichthyans. Coincident with the conquest of land and the physiological changes needed to maintain calcium homeostasis, our expression analyses suggest a change in the expression pattern from gills to kidney. Within amniotes, we identified a traceable sequence signature of three amino acids at the amino-terminal intracellular region that correlates well with both of the duplication events and the phenotype of fast inactivation observed in TRPV6 channels. Electrophysiological recordings and mutagenesis suggest that calcium-induced fast inactivation is an evolutionary innovation that emerged independently from each duplication event. Simulations of molecular dynamics suggest that calcium-induced channel rearrangements are important modulatory regions of TRP channels.

Introduction

Calcium ions (Ca^{2+}) are essential to maintain cellular life; as a consequence, Ca^{2+} homeostasis is highly controlled in all living organisms. TRPV5 and TRPV6 are ion channels that are highly calcium-selective and are members of the Transient Receptor Potential (TRP) gene family(Van Abel et al., 2005). These proteins, expressed at the apical membrane of Ca^{2+} transporting epithelia, serve as entry channels in transepithelial Ca^{2+} transport(Van Abel et al., 2005). As part of the molecular machinery controlling the passage of calcium ions through epithelial barriers, these channels are essential for calcium homeostasis in vertebrates(Bianco et al., 2007; Hoenderop et al., 2003; Van Abel et al., 2005).

The biophysical features of TRPV5 and TRPV6 make them ideally suited to facilitate intestinal absorption and renal reabsorption of Ca^{2+} in mammals(Peng et al., 2017). In agreement with their importance, TRPV6 deficient mice have impaired Ca^{2+} homeostasis, evidenced by poor weight gain, decreased bone mineral density, and reduced fertility(Bianco et al., 2007). In contrast, TRPV5 null mice have less severe physiological consequences(Hoenderop et al., 2003). The calcium selectivity of TRPV5 and TRPV6 is accompanied by different mechanisms of Ca^{2+}-dependent inactivation(Hoenderop et al., 2001), which controls Ca^{2+} entry during the first steps of transcellular transport(Van Abel et al., 2005). One major difference between TRPV5 and TRPV6 rests in how they are distributed among tissues. TRPV5 is predominantly expressed in the distal convoluted tubules (DCT) and connecting tubules (CNT) of the kidney. In contrast, TRPV6 is more broadly expressed; it is found not only in the Ca^{2+} absorbing epithelia of the intestine but in placenta, pancreas, and prostate among others. This suggests that the physiological role of TRPV6 is not limited to the maintenance of Ca^{2+} homeostasis(Peng et al., 2017).

Both TRPV5 and TRPV6 channels have been described in mammals, yet there is only one calcium-selective TRP channel encoded in the genomes of bony fish (TRPV6) and birds

(TRPV6)(Peng, 2011; Qiu and Hogstrand, 2004). It has been suggested that TRPV5 and TRPV6 originated by gene duplication in the last common ancestor of mammals, between 312 and 177 million years ago(Peng, 2011; Saito et al., 2011). Besides these observations, not much else is known about the evolutionary history of the calcium-selective TRP channels in vertebrates. In principle, comparative analysis of calcium-selective TRP channels in representative species of vertebrates should provide valuable information regarding the mode of evolution of genes that are required for calcium homeostasis. Phylogenetic analyses in combination with functional assays should allow inferences regarding their duplicative history, the evolution of function and expression, as well as, the ancestral state of all vertebrates.

Results and Discussion

To understand the evolutionary history of the TRPV5 and TRPV6 genes, we first reconstructed a phylogenetic tree including sequences from species of all major groups of vertebrates. According to our maximum likelihood analyses, the monophyly of the group that includes TRPV5 and TRPV6 sequences from vertebrates is strongly supported (Fig. 1). Synteny analyses provide further support for the monophyly of the clade as genes encoding TRPV5 and TRPV6 are located in a conserved genomic region (Fig. 2). A close inspection of the alignment also supports the monophyly of the clade as several conserved residues can be easily mapped throughout the alignment and gaps introduced by the outgroups (TRPV1-4) are not shared by any of the TRPV5 and TRPV6 proteins (Supplementary Figure 1). Thus, phylogenetic, synteny, and primary sequence analyses provide strong evidence for the monophyly of the TRPV5 and TRPV6 channels in vertebrates.

Within the TRPV5/TRPV6 clade, our phylogenetic analyses suggest not a single but four independent expansion events during the evolutionary history of vertebrates (Fig. 1). The ancestral condition of a single gene copy (referred to here as TRPV5/6) is present in cyclostomes, bony fish, and coelacanths (Fig. 1). However, in chondrichthyans (e.g. sharks, rays,

and chimaeras), the ancestral gene underwent a duplication event, giving rise to an extra copy (Fig. 1). Among tetrapods, our analysis suggests that the repertoire present in mammals, sauropsids, and amphibians originated independently in the ancestor of each group (Fig. 1). Amphibians possess the most diverse repertoire of all vertebrates where four well-supported gene lineages were recovered (Fig. 1). These likely originated in the ancestor of the group that can be traced back to the carboniferous period. Among mammals, the single gene copy present in the ancestor underwent a duplication event, originating a repertoire of two genes (TRPV5 and TRPV6), which have been retained in all major groups (Fig. 1). The case of sauropsids is less straightforward. The single gene copy present in the ancestor of the group also underwent a duplication event originating a repertoire of two genes (Fig. 1). However, during the radiation of the group, TRPV5 was retained in all major lineages whereas TRPV6 was lost in birds (Fig. 1). A comparison of the chicken and crocodile genomic regions provides further support that the gene present in birds corresponds to TRPV5 and not to TRPV6 as it has been previously suggested (Peng, 2011; Saito et al., 2011) as it shows that birds still possess some exons of the TRPV6 gene in their genomes (supplementary fig. 2). Thus, our results provide strong evidence that essential genes required for calcium homeostasis have been duplicated four independent times during the evolutionary history of vertebrates. This observation implies that TRPV5 and TRPV6 genes in mammals, sauropsids, amphibians, and chondrichthyans are not 1:1 orthologs.

From a physiological perspective, our results suggest that the division of labor needed for Ca^{2+} absorption and reabsorption has occurred independently in mammals, sauropsids, amphibians, and chondrichthyans. In mammals this phenomenon is well characterized, while TRPV6 helps in Ca^{2+} absorption, TRPV5 is mainly dedicated to calcium re-absorption in the kidney (Peng et al., 2017; Van Abel et al., 2005). This correlates well with their expression in tissues; while TRPV6 channels are broadly expressed in a variety of tissues (including the kidney, intestine, placenta, pancreas, and prostate among others), TRPV5 is restricted to the distal

convoluted tubule and connecting tubule of the kidney(Peng et al., 2017; Van Abel et al., 2005). In contrast to mammals, much less is known regarding the expression of these genes in other vertebrates; thus, we characterized the transcription profiles of TRPV5 and TRPV6 in representative species of vertebrate (Fig. 3). According to our results, and in support of previous observations in zebrafish(Vanoevelen et al., 2011), marine vertebrates mostly express calcium-selective TRPV channels in their gills, no matter the number of gene copies present in their genomes. The case of chondrichthyans suggests that the expansion of the gene repertoire did not give rise to a pattern of division of labor rather served to increase the number of channels expressed in the gills. Only one of the four gene lineages present in the genome of amphibians is highly expressed in the kidney (Fig. 3), suggesting an association with early adaptations to a terrestrial lifestyle (Mahasen, 2016). In reptiles, both lineages are expressed in the kidney, however TRPV6 was detected in testis as well (Fig. 3). Finally, birds represent an interesting case study as they retained only one of the copies that were present in their ancestor (i.e. TRPV5). As seen in other amniotes, the TRPV5 gene of birds is mainly expressed in the kidney (Fig. 3). Thus, our results show that the expression of calcium-selective TRPV channels in the gills is the ancestral condition of vertebrates. Moreover, it seems that together with the conquest of land, the repertoire of genes not only expanded but also divided the territories of expression. While one of the copies is mainly expressed in kidneys, the other is broadly expressed in a variety of tissues.

The division of labor observed in calcium-selective TRP channels has been accompanied by subtle but important functional adaptations. Given negative membrane potentials, calcium-selective TRP channels permeate calcium ions to the cytoplasm. Together with this, they also exhibit two-phase calcium-dependent inactivation (Hoenderop et al., 2001). The slow component of this inactivation is shared by both channels and is determined by the binding of the Ca^{2+}-Calmodulin complex to the C-terminal region of the channel (Hoenderop et al., 2001;

Nilius et al., 2003; Singh et al., 2018). In contrast, in physiological conditions, rapid inactivation that depends solely on calcium ions is observed only in TRPV6 channels (Hoenderop et al., 2001; Nilius et al., 2002). In support of our evolutionary analyses, whole cell recordings in the presence of 2mM extracellular Ca^{2+} show an absence of fast inactivation in chicken channels (chTRPV5) while this is normally seen in human TRPV5 (hTRPV5) channels (Fig. 4A). Thus, functional and evolutionary evidence strongly suggest that birds retained TRPV5 in their genomes.

Previous studies have identified residues located at the S2-S3 linker (Nilius et al., 2002) and downstream of the transmembrane segment S6 (Suzuki et al., 2002) as important for the rapid inactivation of TRPV6 channels. A close inspection of the S2-S3 linker showed the presence of a loose signature that mirrors with the duplication events that occurred in mammals and, to some extent, reptiles and birds (Fig. 4B). According to the recently published structures (Hughes et al., 2018; Saotome et al., 2016), the S2-S3 loop seems to be conveniently adjacent to the TRP domain helix (TD-helix) and close to an N-terminal helix-loop-helix (HLH) motif. This is interesting given that the TD-helix is a known modulator of TRP channel activity (Gregorio-teruel et al., 2015; Valente et al., 2008) and together with HLF forms a structural triad (Fig. 4C). This triad is supported by a cluster of interactions that have been previously implicated in the modulation of TRP channel activity (Liao et al., 2013; Rosasco and Gordon, 2017; Steinberg et al., 2014). A closer inspection of the alignment used for our phylogenetic reconstruction revealed a second and stronger sequence signature that correlates well with the observed gene duplication events (Fig. 4D). The signature is composed of three amino acids located at the HLH domain in mammals, reptiles, and birds. The presence of these signatures, at two distant locations of the primary sequence and in channels that have originated independently, suggest a strong functional association between the S2-S3 loop and the HLH domain. To test this prediction, we transferred this signature observed at the HLH of the TRPV6 channels (*inactivation signature* 1, IS1) into the TRPV5 channels and describe the inactivation profile by means of whole-cell patch clamp

electrophysiological recordings in the presence of 2mM extracellular Ca^{2+}. In agreement with our prediction, engineered mammalian and avian TRPV5 channels now containing the three-residue inactivation signature of TRPV6 showed a phenotype of calcium-dependent fast inactivation (Figs. 4E and 4F). Furthermore, the process of fast-inactivation is absent in the TRPV5/6 channel of the spotted gar (*Lepisosteus oculatus*; gTRPV5/6) (Fig. 4G and 4H), suggesting that the absence of fast inactivation (i.e the TRPV5 phenotype) represents the ancestral condition of vertebrates. Similar to our previous experiment, introducing IS1 in the single copy gene of the spotted gar was enough to transfer the fast inactivation phenotype to the fish channel (Fig. 4G and 4H). The anole lizard (*Anolis carolinensis,* aTRPV5) represents a valuable opportunity provided by a natural mutant to understand the molecular basis of the inactivation. In this case, the amino acid signature at the S2-S3 linker (*inactivation signature* 2, IS2) suggests that the anole lizard TRPV5 channel should be capable of inactivation (Fig. 4B), whereas IS1 suggests the opposite (Fig. 4D). Electrophysiological recordings showed that while the anole lizard TRPV6 (aTRPV6) channel is not capable of inactivation (in contrast to that of mammals), aTRPV5 elicits modest inactivation where nearly 20% of the residual current is lost at steady states (Fig. 4G and 4H). We then explored whether this modest inactivation was correlated with the "inverted" IS2 signature present in the anole lizard TRPV5 channel. By reversing the natural oddity to what the analysis suggested should be the correct signature for lack of inactivation (I415V, F420Y); we were able to completely suppress inactivation (Fig. 4G and 4H). Overall, this confirm previous observations where mutations introduced in the S2-S3 linker of the mammalian TRPV6 channels significantly delayed inactivation (Nilius et al., 2002). On the other hand, the introduction of IS1 in the anole lizard TRPV5 channel produced a robust inactivation phenotype similar to the mammalian counterpart regardless of the presence of the inactivation signature at the linker (Fig. 4G and 4H). Thus, our results strongly suggest that the coordinated activity of both the HLH motif and the S2-S3 linker determine the phenotype of fast inactivation observed in TRPV6 channels.

To explore whether changes in the elements of the HLH/S2-S3 linker/TD-helix triad correlated with the phenotypes observed, we studied the primary sequences in these three different protein regions. We observed that both the HLH and the S2-S3 linker seem to be more conserved in mammals and sauropsids and more variable in amphibians and fish (Fig. 5A). In contrast, the consensus sequence corresponding to the TD-helix is relatively conserved in all examined groups, as expected for *bona fide* TRPV channels (Fig. 5A). In mammals and sauropsids, the channels possess both inactivation phenotypes, and coincidently the HLH domain has a scaffold of conserved amino acids around the critical residues modulating the fast inactivation phenotype (Fig. 5A, green box, blue asterisks). This scaffold is different from that observed in amphibians and fish (Figure 5A, green box). Moreover, the signature residues aspartic acid (position 8) and valine (position 12) are well conserved in amphibians and fish suggesting that developing fast inactivation is not possible (Fig. 5A, blue asterisks). On the other hand, a similar but less strong pattern is detectable at the S2-S3 linker. Here, mammals and sauropsids have a more conserved set of amino acids around the residues defining the phenotype of fast inactivation (Fig. 5A, yellow box, pink asterisks). Moreover, in amphibians and fish, there is conservation of just one of the linker's signature amino acids associated with fast inactivation (tyrosine at position 12). Taken together, our analyses suggest that the S2-S3 linker's ability to modulate coordination among elements of the structural triad probably precedes the phenotype of fast inactivation itself (Fig. 4B and Fig. 5A). Additionally, the necessary requirement to accomplish calcium-dependent fast inactivation was to engineer the HLH domain in one of the duplicated genes, a scenario we can only observe in contemporary species that live in terrestrial environments.

Amino acids at or close to the HLH region have been implicated in the modulation of temperature-activation in TRPV1 and TRPV3 (Liu and Qin, 2017; Yao et al., 2011) and chemical-activation in TRPA1 (Saito et al., 2014). At the same time, the region close to the S2-S3 linker has been shown to have coordinated calcium ions in TRPM4 and TRPM2 (Autzen et al.,

2018; Huang et al., 2018). To explore whether the HLH/S2-S3 linker/TD-helix triad might function as a calcium-binding region in TRPV5 and TRPV6 channels, we used the structural information publically available to perform a more detailed analysis of the region. An initial inspection of the electrostatics of the soluble domains of the channels suggests the presence of electronegative cavities close to the S2-S3 linker and the HLH domain (Fig. 5B). Moreover, these electronegative regions are dense in oxygen atoms, suggesting the presence of putative calcium binding sites (Fig. 5C). Thus, we performed short (100 ns) molecular dynamics simulations with 150 mM Ca^{2+} in solution to explore whether these cavities, around the region defined by the structural triad, are able to coordinate calcium ions. Simulations performed in TRPV5 (rbTRPV5, PDB: 6B5V(Hughes et al., 2018)) and TRPV6 (rTRPV6, PDB: 5IWK(Saotome et al., 2016)) allowed us to identify three putative calcium-binding sites associated with the HLH domain/S2-S3 linker/TD-helix region (Figure 5D). Although these putative calcium-binding sites share amino acid positions between rbTRPV5 (E288, E289, D406) and rTRPV6 (D287, D288, D405), the number of amino acids coordinating calcium is larger in rTRPV6 (Fig. 5D; supplementary figure 3). Our simulations suggest that the channels might rearrange differently upon calcium binding, thus originating differences in the relative position of the S2-S3 linker with respect to the TRP domain helix (supplementary videos 1 and 2). Taken together, our structural analysis suggests that the coordinated activity of the S2-S3 linker and HLH domain evolved to originate fast inactivation by introducing innovations at the HLH domain that direct calcium binding and reshape the interactions of the triad. Additionally, the degrees of freedom of the S2-S3 linker are likely important in modulating the state of the channel gate.

In summary, our study shows that the evolutionary history of TRPV5 and TRPV6 channels in vertebrates is dynamic. We propose that the ancestral condition of vertebrates included a single copy gene that encoded a non-fast inactivation channel. This gene could have had properties similar to the ones observed in contemporary species of cyclostomes, bony fish, and coelacanths, including high selectivity for divalent ions(Qiu and Hogstrand, 2004). This

would suggest that calcium selectivity in these channels precedes calcium-dependent fast-inactivation. During the evolutionary history of vertebrates, chondrichthyans, amphibians, sauropsids, and mammals independently originated a more diverse repertoire of calcium-selective TRP channels. The independent origin of genes seems not to be uncommon in nature and implies that gene repertoires are not directly comparable, as they do not have the same evolutionary origin (Opazo and Zavala, 2018). It has been shown that the convergence of phenotypes could be reached by different pathways (Natarajan et al., 2016), thus the reinvention of these calcium-selective TRP channels opens an opportunity to understand in more detail the diversity of mechanisms associated with transepithelial Ca^{2+} transport. In terrestrial vertebrates, the origin of new lineages of TRPV channels is associated with division of the expression territories and origin of the fast inactivation phenotype. Interestingly, the change in the pattern of expression not only correlates with a clear expansion to the kidney and the intestine where calcium absorption/reabsorption takes place but coincides with the environmental conditions that the species inhabit. Among amniotes, duplicated copies are differentiated by specific amino acid substitutions in both the HLH domain and the S2S-S3 linker, and these amino acid substitutions could be strongly correlated with the fast inactivation phenotype. The presence of conserved residues in the HLH domain leads to differences in calcium coordination and inter-domain interactions within the structural HLH domain/S2-S3 linker/TD-helix triad, highlighting the significance of the region for TRP channel function. Subtle differences in the coordination of this triad might extend to other channels of the TRP family and might represent one of the molecular cornerstones of TRP channel inner workings.

Material and Methods

Sequence data and phylogenetic analyses

We retrieved calcium-selective TRP channel sequences from representative species of all major groups of vertebrates. Our sampling included species from mammals, birds, reptiles, amphibians, coelacanths, holostean fish, teleost fish, chondrichthyans and cyclostomes (Supplementary Table 1). Protein sequences were obtained from the Orthologous MAtrix project (OMA)(Altenhoff et al., 2018). In cases where the species were not included in the OMA project, we searched the NCBI database (refseq_genomes, htgs, and wgs) using tbalstn(Altschul et al., 1990) with default settings. Protein sequences were aligned using the FFT-NS-1 strategy from MAFFT v.7(Katoh and Standley, 2013). We used the proposed model tool of IQ-Tree v1.6.6(Trifinopoulos et al., 2016) to select the best-fitting model of amino acid substitution (JTT + F + R6). We employed maximum-likelihood to obtain the best tree using the program IQ-Tree v1.6.6(Trifinopoulos et al., 2016). Node support was assessed with 1000 bootstrap pseudoreplicates using the ultrafast routine. TRPV1, TRPV2, TRPV3, TRPV4 and TRPA1 were used as outgroups.

Assessment of Conserved Synteny

We examined genes found upstream and downstream of the TRPV5 and TRPV6 genes in species representative of all major groups of vertebrates. We used estimates of orthology and paralogy derived from the EnsemblCompara database(Herrero et al., 2016); these estimates were obtained from an automated pipeline that considers both synteny and phylogeny to generate orthology mappings. These predictions were visualized using the program Genomicus v93.01(Louis et al., 2014). Our assessments were performed in humans (*Homo sapiens*), chicken (*Gallus gallus*), American alligator (*Alligator mississippiensis*), Chinese softshell turtle (*Pelodiscus sinensis*), anole lizard (*Anolis carolinensis*), African clawed frog (*Xenopus laevis*), coelacanth (*Latimeria chalumnae*), spotted gar (*Lepisosteus oculatus*), zebrafish (*Danio rerio*), and *Callorhinchus milii*, the elephant fish, which is sometimes labeled as elephant shark. In the case of the elephant fish, and

American alligator, flanking genes were examined using the Entrez gene database from NCBI(Maglott et al., 2011).

Expression analysis

TRPV5 and TRPV6 expression was measured from a representative sample of vertebrates including elephant fish (*Callorhinchus milii)*, spotted gar (*Lepisosteus oculatus*), African clawed frog (*Xenopus laevis*), anole lizard (*Anolis carolinensis*), chicken (*Gallus gallus*) and human (*Homo sapiens*). RNASeq data from a spectrum of tissues including brain, heart, intestine, kidney, liver, muscle, ovary, testis, gills and skin, were gathered from the Short Read Archive (SRA). Accession numbers for species and tissue specific libraries can be found in Supplemental Table 2. For all species except the elephant shark and the African clawed frog, we used Ensembl predicted gene sequences for gene expression references. Elephant fish and *X. laevis* cDNA sequences were collected from NCBI. To remove redundancy from libraries, all predicted TRPV5 and TRPV6 transcripts were removed from each library and replaced with our annotations. Adapter sequences were removed from the RNASeq reads using Trimmomatic 0.38(Bolger et al., 2014), and reads were filtered for quality using the parameters HEADCROP:1, LEADING:30, TRAILING:30, SLIDINGWINDOW:5:30, and MINLEN:50. We used RSEM 1.3.1(Li and Dewey, 2011) to map reads with Bowtie 1.2.2(Langmead et al., 2009) and to estimate gene expression in units of TPM.

Molecular Biology, Cell Culture, and Transfection

Open Reading Frames (ORF) encoding the different channels analyzed [Spotted gar TRPV5/6 (gTRPV5/6) WT, gTRPV5 V294LC300T (IS-1), anole lizard TRPV5 (aTRPV5) WT, aTRPV5 E293DF297LS303T (IS-1), aTRPV5 I415VF420Y (IS-2) anole lizard TRPV6 (aTRPV6) WT, chicken TRPV5 (chTRPV5) WT, chTRPV5 E290DF294LS300T (IS-1), human TRPV5 (hTRPV5) WT, hTRPV5 E288DF292LS298T (IS-1) and human TRPV6 (hTRPV6) WT] were obtained from GenScript Corporation (Nanjing, China) and were inserted in a pcDNA3.1(+)

vector. HEK 293T cells were grown in DMEM-F12 medium containing 10% (v/v) bovine fetal serum at 37ºC in a humidity-controlled incubator with 5% (v/v) CO_2. HEK 293T cells were transiently co-transfected with the different clones analyzed and peGFP-N1 to allow for their identification.

Electrophysiology and solutions

Whole-cell currents were measured with an Axopatch-200B amplifier. We used borosilicate pipettes (o.d. 1.5mm, i.d. 0.86mm, Warner Instruments, Hamden, CT) with resistance of 2 to 4.0 MΩ to form seals with access resistance between 2 and 6 GΩ. Macroscopic currents were recorded in response to a voltage step protocol from zero to -160 mV. Inactivation was analyzed in a time window of 60 ms. Recordings were digitized at 10KHz and filtered at 5KHz using a digitada 1320 (Molecular Devices, LLC, California). The analysis was performed using Clampfit 10.3 (Molecular Devices, LLC, California). Fast inactivation was assessed by computing the residual currents, defined as the ratio of the current value at the end of the negative pulse over the current at the beginning of the voltage pulse (Derler et al., 2006). The standard extracellular solution (Ringer-Na^+) contained (in mM) 140 NaCl, 5 KCl, 2 $CaCl_2$, 2$MgCl_2$, 8 glucose and 10 HEPES, at pH 7.4 adjusted with NaOH. The standard internal (pipette) solution contained (in mM) 105 CsF, 35 NaCl, 10 EGTA and 10 HEPES, at ph 7.4 adjusted with CsOH. All of the experiments were performed at room temperature (20 to 25ºC).

Statistical Analysis

Data are expressed as mean ± S.E. Overall statistical significance was determined using analyses of variance (ANOVA one way and two ways) with a Bonferroni post-test. For all conditions, the average was obtained from at least seven independent experiments. Outliers were defined using GraphPad QuickCalcs (https://www.graphpad.com/quickcalcs/Grubbs1.cfm), and outliers were removed from the analysis.

Bioinformatics and Molecular Dynamics Simulations

Three-dimensional structures of rat TRPV6 (rTRPV6, PDB: 5IWK) (Saotome et al., 2016) and rabbit TRPV5 (rbTRPV5, PDB: 6B5V) (Hughes et al., 2018) were prepared at pH 7.0 and subjected to energy minimization in a vacuum using the Maestro-Schrödinger suite (Schrödinger Release 2018-2: Maestro, Schrödinger, LLC, New York, NY, 2018). The channels were embedded into a pre-equilibrated POPC lipid bilayer in an orthorhombic box with periodic borders. This was filled with Single Point Charge (SPC) water molecules and an ionic concentration of 150 mM Ca^{2+} and Cl^{-} ions. Full atom Molecular Dynamics (MD) simulations of 100ns were performed in triplicate in a NPT ensemble (P = 1 atm, T = 310 K) using Desmond (Bowers et al., 2006) and OPLS v.2005 force field. Structures were collected every 0.12 nanoseconds during the MD simulations; thus, 835 frames were obtained *per* simulation. The electrostatic potential of the region of interest was calculated using the ABPS plugin (version 1.3) of VMD(Humphrey et al., 1996). Protein residues interacting with calcium ions were identified taking into account a maximal distance of 2.5 Å and the three simulations together.

Figure legends

Figure 1. Maximum likelihood tree depicting evolutionary relationships among the TRPV5 and TRPV6 genes of vertebrates. Numbers on the nodes represent maximum likelihood ultrafast bootstrap support values. TRPV1, TRPV2, TRPV3, TRPV4 and TRPA1 were used as outgroups.

Figure 2. Patterns of conserved synteny in the chromosomal regions that harbor the TRPV5 and TRPV6 genes. Asterisks indicate that the orientation of the genomic piece is from 3´ to 5´, gray lines represent genes that do not contribute to conserved synteny whereas diagonals indicate that the chromosomal pieces are not continuous.

Figure 3. Comparative expression profiles of vertebrate TRPV5/6 genes across multiple tissues. mRNA levels were estimated from public RNA-Seq libraries. Asterisks indicate data were not available for that species and tissue, and hashes indicate the tissue was absent.

Figure 4. Specific amino acid replacements at the HLH domain and S2-S3 linker correlate with the fast inactivation phenotype. (A) Normalized whole cell current traces recorded from transiently transfected HEK-293T cells expressing human TRPV5 and TRPV6 (hTRPV5 WT; hTRPV6 WT, respectively) and chicken TRPV5 (chTRPV5 WT). Voltage protocol and ionic conditions are indicated. (B) Amino acid sequence alignment of the S2-S3 linker of the TRPV5, TRPV6 and TRPV5/6 channels. Non-inactivating TRPV5 channels show conserved residues (light blue) that differ from residues present in TRPV6 channels (light purple). (C) Structure of one subunit of the rat TRPV6 channel (rTRPV6; PDB: 5IWK)(Saotome et al., 2016) showing the structural triad HLH domain (green), S2-S3 linker (yellow) and TD-helix (orange). (D)

Amino acid sequence alignment of the HLH domain. Conserved residues in TRPV5/6 (red), TRPV5 (light blue) and TRPV6 (light purple) are highlighted. (E) Normalized whole cell current traces recorded from the human (hTRPV5-IS1; E288D; F292L; S298T) and chicken TRPV5 (chTRPV5-IS1; E290D; F294L; S300T) channels containing the three-residue inactivation signature of TRPV6 and human TRPV6 channel (hTRPV6 WT). (F) Pooled data comparing the residual currents (see methods). (G) Normalized whole cell current traces, recorded from the anole lizard TRPV5 channel wild type (aTRPV5 WT), containing the three-residue inactivation signature of TRPV6 (aTRPV5-IS1; E293D; F297L; S303T), containing the amino acid signature at the S2-S3 linker (aTRPV5-IS2; I415V; F420Y), the TRPV6 channel wild type (aTRPV6 WT), and the spotted gar TRPV5/6 channel wild type (gTRPV5/6 WT) and containing the three-residue inactivation signature of TRPV6 (gTRPV5/6-IS1; V294L; C300T). (H) Pooled data comparing the residual currents. All of the current traces were recorded in presence of 2mM extracellular Ca^{2+} and in response to a voltage pulse at -160mV for 60ms from Vh=0mV.

Figure 5. Structural triad formed by the HLH domain, S2S3 linker, and TRP helix could constitute a calcium binding pocket. (A) Residue conservation (in blue shades) for the components of the structural triad. HLH domain (green), S2-S3 linker (yellow), and TD-Helix (orange) are depicted along with the conservation of two sets of mammalian and sauropsid (gray subset) data and amphibian and fish data (black subset). Residues highlighted in the S2-S3 linker (light pink shades and asterisk) and the HLH domain (blue shades and asterisk) have been directly related to the inactivation phenotype. (B) Electrostatic potential profile of the pocket formed by the HLH domain, S2-S3 linker, and TD helix. (C) Density of exposed oxygen in the

region of interest. (D) Presence of three putative calcium-binding sites in the region formed by the HLH domain (green), S2-S3 linker (yellow) and TD-helix (orange) in the rbTRPV5 and rTRPV6 channels.

References

Altenhoff AM, Glover NM, Train C-M, Kaleb K, Vesztrocy AW, Dylus D, De Farias TM, Zile K, Stevenson C, Long J, Redestig H, Gonnet GH, Dessimoz C. 2018. The OMA orthology database in 2018 : retrieving evolutionary relationships among all domains of life through richer web and programmatic interfaces. *Nucleic Acids Res* **46**:477–485. doi:10.1093/nar/gkx1019

Altschul SF, Gish W, Miller W, Myers EW, Lipman DJ. 1990. Basic Local Alignment Search Tool. *J Mol Biol* **215**:403–410.

Autzen HE, Myasnikov AG, Campbell MG, Asarnow D, Julius D, Cheng Y. 2018. Structure of the human TRPM4 ion channel in a lipid nanodisc. *Science (80-)* **359**:228–232. doi:10.1126/science.aar4510.Structure

Bianco SD, Peng J-B, Takanaga H, Suzuki Y, Crescenzi A, Kos CH, Zhuang L, Freeman MR, Gouveia CH, Wu J, Luo H, Mauro T, Brown EM, Hediger MA. 2007. Marked Disturbance of Calcium Homeostasis in Mice With Targeted Disruption of the Trpv6 Calcium Channel Gene HHS Public Access. *J Bone Min Res J Bone Min Res* **22**:274–285. doi:10.1359/jbmr.061110

Bolger AM, Lohse M, Usadel B. 2014. Genome analysis Trimmomatic : a flexible trimmer for Illumina sequence data. *Bioinformatics* **30**:2114–2120. doi:10.1093/bioinformatics/btu170

Bowers K, Chow E, Xu H, Dror R, Eastwood M, Gregersen B, Klepeis J, Kolossvary I, Moraes M, Sacerdoti F, Salmon J, Shan Y, Shaw D. 2006. Scalable Algorithms for Molecular Dynamics Simulations on Commodity ClustersSC '06: Proceedings of the 2006

ACM/IEEE Conference on Supercomputing. pp. 43–43. doi:10.1109/SC.2006.54

Derler I, Hofbauer M, Kahr H, Fritsch R, Muik M, Kepplinger K, Hack ME, Moritz S, Schindl R, Groschner K, Romanin C. 2006. Dynamic but not constitutive association of calmodulin with rat TRPV6 channels enables fine tuning of Ca2+-dependent inactivation. *J Physiol* **577**:31–44. doi:10.1113/jphysiol.2006.118661

Gregorio-teruel L, Valente P, Liu B, Fernandez-Ballester G, Qin F, Ferrer-Montiel A. 2015. The Integrity of the TRP Domain Is Pivotal for Correct TRPV1 Channel Gating **109**:529–541. doi:10.1016/j.bpj.2015.06.039

Herrero J, Matthieu M, Beal K, Fitzgerald S, Gordon L, Pignatelli M, Vilella AJ, Searle SMJ, Amode R, Brent S, Spooner W, Kulesha E, Yates A, Flicek P. 2016. Database update Ensembl comparative genomics resources. *Database* 1–17. doi:10.1093/database/bav096

Hoenderop JG, Vennekens R, Müller D, Prenen J, Droogmans G, Bindels RJ, Nilius B. 2001. Function and expression of the epithelial Ca(2+) channel family: comparison of mammalian ECaC1 and 2. *J Physiol* **537**:747–761. doi:10.1111/j.1469-7793.2001.00747.x

Hoenderop JGJ, Van Leeuwen JPTM, Van Der Eerden BCJ, Kersten FFJ, Van Der Kemp AWCM, Mérillat AM, Waarsing JH, Rossier BC, Vallon V, Hummler E, Bindels RJM. 2003. Renal Ca2+ wasting, hyperabsorption, and reduced bone thickness in mice lacking TRPV5. *J Clin Invest* **112**:1906–1914. doi:10.1172/JCI200319826

Huang Y, Winkler PA, Sun W, Lü W, Du J. 2018. Architecture of the TRPM2 channel and its activation mechanism by ADP-ribose and calcium. doi:10.1038/s41586-018-0558-4

Hughes TET, Lodowski DT, Huynh KW, Yazici A, Del Rosario J, Kapoor A, Basak S, Samanta A, Han X, Chakrapani S, Zhou ZH, Filizola M, Rohacs T, Han S, Moiseenkova-Bell VY. 2018. Structural basis of TRPV5 channel inhibition by econazole revealed by cryo-EM. *Nat Struct Mol Biol* **25**:53–60. doi:10.1038/s41594-017-0009-1

Humphrey W, Dalke A, Schulten K. 1996. VMD: Visual molecular dynamics. *J Mol Graph.* doi:10.1016/0263-7855(96)00018-5

Katoh K, Standley DM. 2013. MAFFT Multiple Sequence Alignment Software Version 7 : Improvements in Performance and Usability Article Fast Track **30**:772–780. doi:10.1093/molbev/mst010

Langmead B, Trapnell C, Pop M, Salzberg SL. 2009. Ultrafast and memory-efficient alignment of short DNA sequences to the human genome. *Genome Biol* **10**:R25. doi:10.1186/gb-2009-10-3-r25

Li B, Dewey CN. 2011. RSEM : accurate transcript quantification from RNA-Seq data with or without a reference genome. *BMC Bioinformatics* **12**:323. doi:10.1186/1471-2105-12-323

Liao M, Cao E, Julius D, Cheng Y. 2013. Structure of the TRPV1 ion channel determined by electron cryo-microscopy. *Nature* **504**:107–112. doi:10.1038/nature12822

Liu B, Qin F. 2017. Single-residue molecular switch for high-temperature dependence of vanilloid receptor TRPV3 1–6. doi:10.1073/pnas.1615304114

Louis A, Thi N, Nguyen T, Muffato M, Crollius HR. 2014. Genomicus update 2015 : KaryoView and MatrixView provide a genome-wide perspective to multispecies comparative genomics. *Nucleic Acids Res* 1–8. doi:10.1093/nar/gku1112

Maglott D, Ostell J, Pruitt KD, Tatusova T. 2011. Entrez Gene : gene-centered information at NCBI. *Nucleic Acids Res* **39**:52–57. doi:10.1093/nar/gkq1237

Mahasen LMA. 2016. Anatomy Physiology & Biochemistry Evolution of the Kidney **1**:1–6.

Natarajan C, Hoffmann FG, Weber RE, Fago A, Witt CC, Storz JF. 2016. Predictable convergence in hemoglobin function has unpredictable molecular underpinnings **354**:336–340.

Nilius B, Prenen J, Hoenderop JGJ, Vennekens R, Hoefs S, Freek Weidema A, Droogmans G, Bindels RJM. 2002. Fast and slow inactivation kinetics of the Ca2+ channels ECaC1 and ECaC2 (TRPV5 and TRPV6): Role of the intracellular loop located between transmembrane segments 2 and 3. *J Biol Chem* **277**:30852–30858. doi:10.1074/jbc.M202418200

Nilius B, Weidema F, Prenen J, Hoenderop JGJ, Vennekens R, Hoefs S, Droogmans G, Bindels RJM. 2003. The carboxyl terminus of the epithelial Ca(2+) channel ECaC1 is involved in Ca(2+)-dependent inactivation. *Pflugers Arch* **445**:584–588. doi:10.1007/s00424-002-0923-9

Opazo JC, Zavala K. 2018. Phylogenetic evidence for independent origins of GDF1 and GDF3 genes in anurans and mammals **1**:13595. doi:10.1038/s41598-018-31954-w

Peng J-B. 2011. TRPV5 and TRPV6 in Transcellular Ca2+ Transport: Regulation, Gene Duplication, and Polymorphisms in African Populations In: Islam MS, editor. Transient Receptor Potential Channels, Advances in Experimental Medicine and Biology. Springer Netherlands. pp. 239–275. doi:10.1007/978-94-007-0265-3

Peng J-B, Suzuki Y, Gyimesi G, Hediger MA. 2017. TRPV5 and TRPV6 calcium-selective channels In: Eichberg JJ, Zhu MX, editors. Calcium Entry Channels in Non-Excitable Cells. FL. pp. 241–274.

Qiu A, Hogstrand C. 2004. Functional characterisation and genomic analysis of an epithelial calcium channel (ECaC) from pufferfish, Fugu rubripes. *Gene* **342**:113–123. doi:10.1016/j.gene.2004.07.041

Rosasco MG, Gordon SE. 2017. TRP Channels. What Do They Look Like? In: TLR E, editor. Neurobiology of TRP Channels. Boca Raton (FL).

Saito S, Banzawa N, Fukuta N, Saito CT, Takahashi K, Imagawa T, Ohta T, Tominaga M. 2014. Heat and Noxious Chemical Sensor , Chicken TRPA1 , as a Target of Bird Repellents and Identification of Its Structural Determinants by Multispecies Functional Comparison **31**:708–722. doi:10.1093/molbev/msu001

Saito S, Fukuta N, Shingai R, Tominaga M. 2011. Evolution of Vertebrate Transient Receptor Potential Vanilloid 3 Channels : Opposite Temperature Sensitivity between Mammals and Western Clawed Frogs. *Plos Genet* **7**. doi:10.1371/journal.pgen.1002041

Saotome K, Singh AK, Yelshanskaya M V., Sobolevsky AI. 2016. Crystal structure of the epithelial calcium channel TRPV6. *Nature* 1–19. doi:10.1038/nature17975

Singh AK, Saotome K, McGoldrick LL, Sobolevsky AI. 2018. Structural bases of TRP channel TRPV6 allosteric modulation by 2-APB. *Nat Commun* **9**:1–11. doi:10.1038/s41467-018-04828-y

Steinberg X, Lespay-Rebolledo C, Brauchi S. 2014. A structural view of ligand-dependent activation in thermoTRP channels. *Front Physiol* **5 MAY**:1–14. doi:10.3389/fphys.2014.00171

Suzuki M, Ohki G, Ishibashi K, Imai M. 2002. A single amino acid mutation results in a rapid inactivation of epithelial calcium channels. *Biochem Biophys Res Commun* **291**:278–85. doi:10.1006/bbrc.2002.6416

Trifinopoulos J, Nguyen L, Haeseler A Von, Minh BQ. 2016. W-IQ-TREE : a fast online phylogenetic tool for maximum likelihood analysis. *Nucleic Acids Res* **44**:232–235. doi:10.1093/nar/gkw256

Valente P, Garcia-Sanz N, Gomis A, Fernandez-Carvajal A, Fernandez-Ballester G, Viana F, Belmonte C, Ferrer-Montiel A. 2008. Identification of molecular determinants of channel gating in the transient receptor potential box of vanilloid receptor I. *FASEB J* **22**:3298–3309. doi:10.1096/fj.08-107425

Van Abel M, Hoenderop JGJ, Bindels RJM. 2005. The epithelial calcium channels TRPV5 and TRPV6: Regulation and implications for disease. *Naunyn Schmiedebergs Arch Pharmacol* **371**:295–306. doi:10.1007/s00210-005-1021-2

Vanoevelen J, Janssens A, Huitema LF a, Hammond CL, Metz JR, Flik G, Voets T, Schulte-Merker S. 2011. Trpv5/6 is vital for epithelial calcium uptake and bone formation. *FASEB J* **25**:3197–3207. doi:10.1096/fj.11-183145

Yao J, Liu B, Qin F. 2011. Modular thermal sensors in temperature-gated transient receptor potential (TRP) channels **2011**. doi:10.1073/pnas.1105196108

Acknowledgments

This work was supported by Anillo Científico ACT-1401, Centro Interdisciplinario de Estudios del Sistema Nervioso (CISNe-UACh), UACh Program for Cell Biology to SEB. Millennium Nucleus of Ion Channels Associated Diseases (MiNICAD), Iniciativa Científica Milenio, Ministry of Economy, Development and Tourism, Chile to SEB and WG. Fondo Nacional de Desarrollo Científico y Tecnológico (FONDECYT 1160627) to JCO and CONICYT 21150220 to LF-A. This work was also supported by the U.S. Dept. of Education, HSI STEM grant P031C110114 – 15.

Contributions

LF-A performed sequence analysis, electrophysiology, and MD simulations. KZ and CKC mine sequences and performed phylogenetic analyses. MWV performed expression analyses. DB performed MD simulations. LFA, SEB, JCO, and WG designed experiments and analyzed data. SEB and JCO wrote the manuscript.

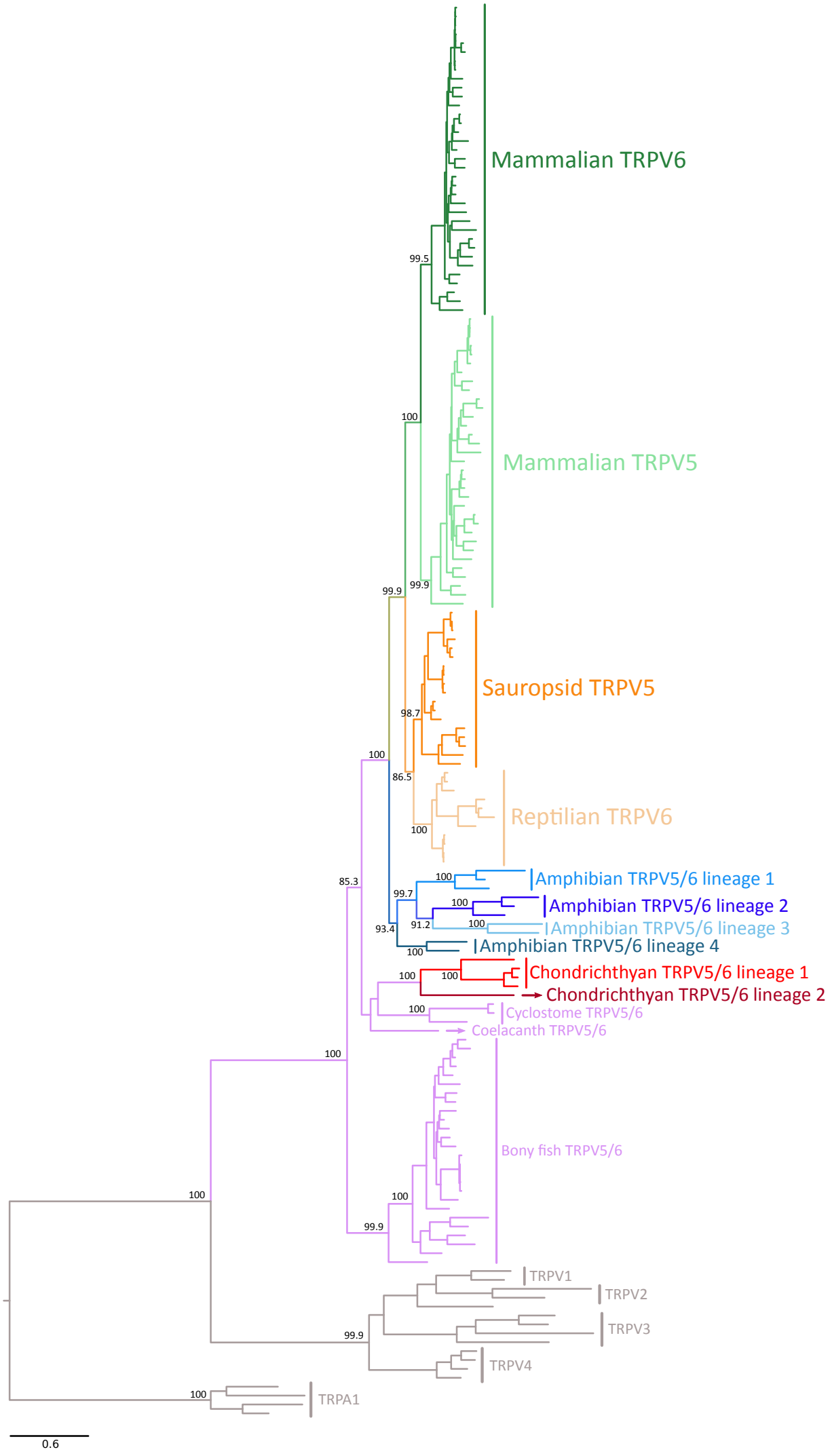
Mammalian TRPV6
Mammalian TRPV5
Sauropsid TRPV5
Reptilian TRPV6
Amphibian TRPV5/6 lineage 1
Amphibian TRPV5/6 lineage 2
Amphibian TRPV5/6 lineage 3
Amphibian TRPV5/6 lineage 4
Chondrichthyan TRPV5/6 lineage 1
Chondrichthyan TRPV5/6 lineage 2
Cyclostome TRPV5/6
Coelacanth TRPV5/6
Bony fish TRPV5/6
TRPV1
TRPV2
TRPV3
TRPV4
TRPA1
99.5
100
99.9
99.9
98.7
100
86.5
100
85.3
100
99.7
100
91.2
100
93.4
100
100
100
100
100
100
100
99.9
100
99.9
100
0.6

Mammals
Birds
Crocodiles
Turtles
Squamates
Amphibians
Coelacanths
Holostean fish
Teleost fish
Cartilaginous fish
TRBC2
TRBV
EPHB6
TRPV6
TRPV5
KEL
GSTK1
TMEM139
CASP2
x5
Human Chr7
Chicken Chr1
American alligator NW_017710106.1*
Chinese turtle JH205551
Anole lizard GL343391/GL343499
African clawed frog Ch7L*
Coelacanth JH127253
Spotted gar LG26*
Zebrafish Chr16
Elephant fish NW_006890063

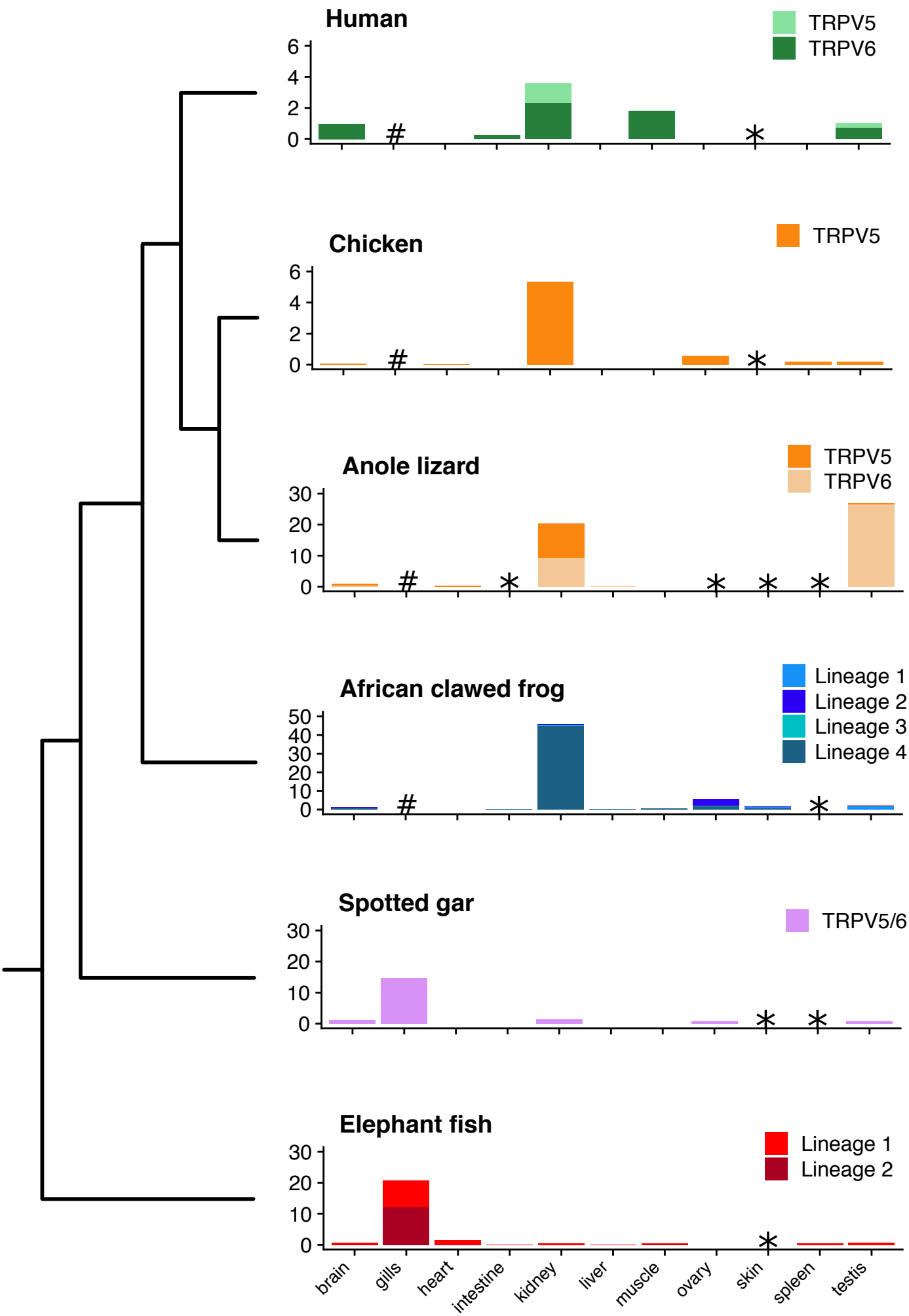
Human
TRPV5
TRPV6
Chicken
TRPV5
Anole lizard
TRPV5
TRPV6
African clawed frog
Lineage 1
Lineage 2
Lineage 3
Lineage 4
Spotted gar
TRPV5/6
Elephant fish
Lineage 1
Lineage 2
brain
gills
heart
intestine
kidney
liver
muscle
ovary
skin
spleen
testis

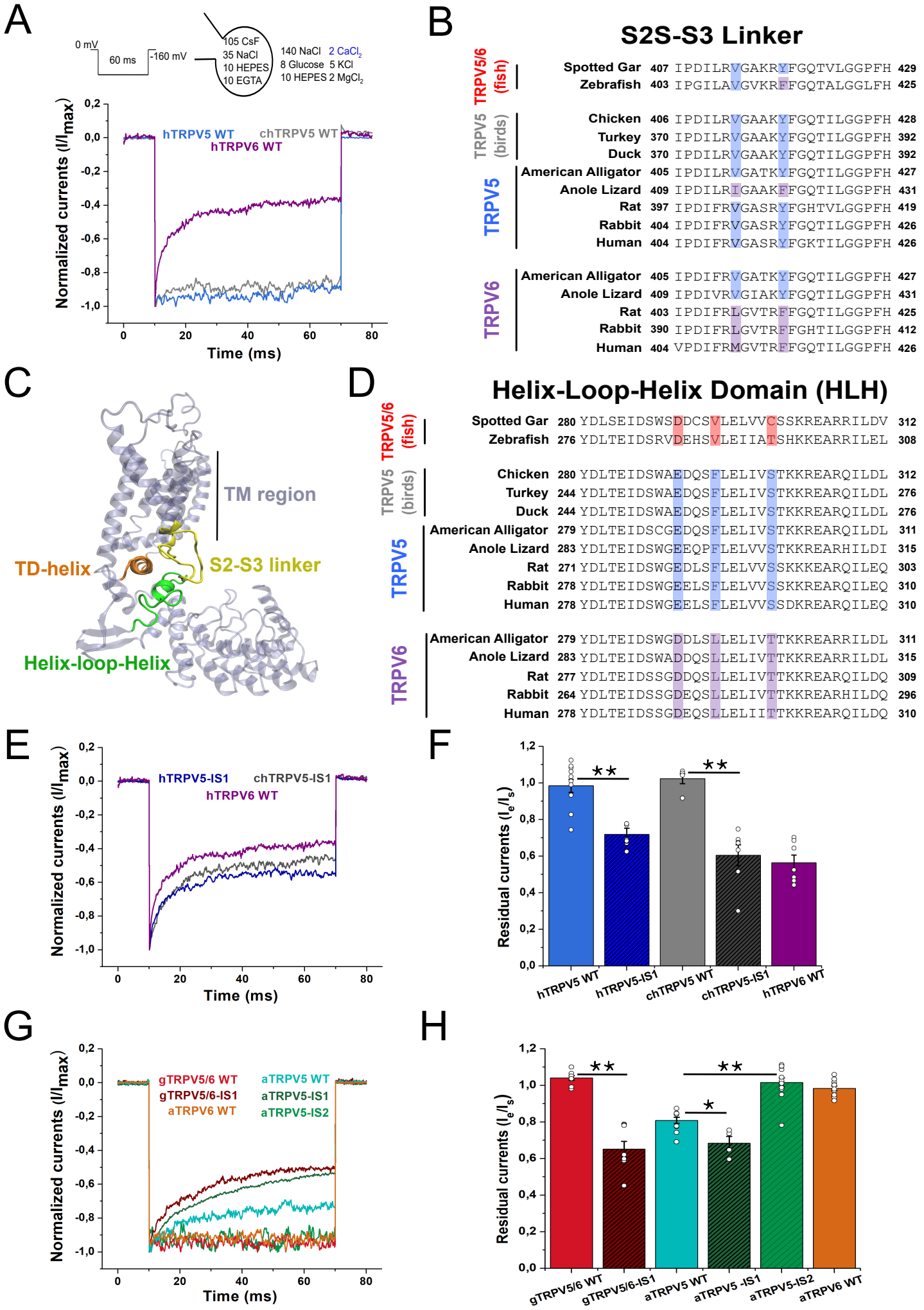

Figure 4. Flores et al.

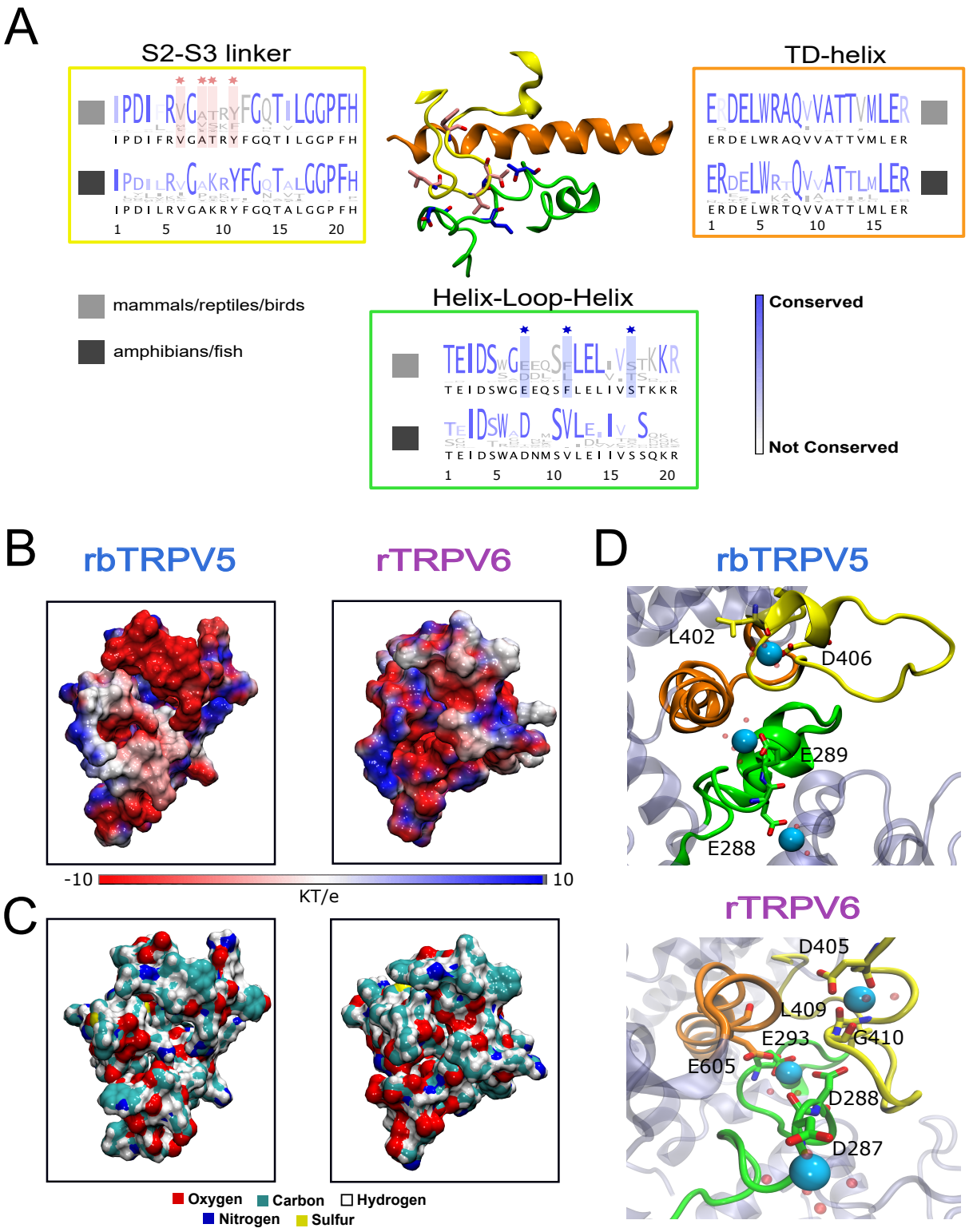

Figure 5. Flores et al.